

# Noninvasive Blood Glucose Monitoring Using Spatiotemporal ECG and PPG Feature Fusion and Weight-Based Choquet Integral Multimodel Approach

Jingzhen Li<sup>ID</sup>, Member, IEEE, Jingjing Ma, Olatunji Mumini Omisore<sup>PD</sup>, Senior Member, IEEE, Yuhang Liu, Huajie Tang, Pengfei Ao, Yan Yan, Member, IEEE, Lei Wang, Member, IEEE, and Zedong Nie<sup>ID</sup>, Member, IEEE

**Abstract**—change of blood glucose (BG) level stimulates the autonomic nervous system leading to variation in both human's electrocardiogram (ECG) and photoplethysmogram (PPG). In this article, we aimed to construct a novel multimodal framework based on ECG and PPG signal fusion to establish a universal BG monitoring model. This is proposed as a spatiotemporal decision fusion strategy that uses weight-based Choquet integral for BG monitoring. Specifically, the multimodal framework performs three-level fusion. First, ECG and PPG signals are collected and coupled into different pools. Second, the temporal statistical features and spatial morphological features in the ECG and PPG signals are extracted through numerical analysis and residual networks, respectively. Furthermore, the suitable temporal statistical features are determined with three feature selection techniques, and the spatial morphological features are compressed by deep neural networks (DNNs). Lastly, weight-based Choquet integral multimodel fusion is integrated for coupling different BG monitoring algorithms based on the temporal statistical features and spatial morphological features. To verify the feasibility of the model, a total of 103 days of ECG and PPG signals encompassing 21 participants were collected in this article. The BG levels of participants ranged between 2.2 and 21.8 mmol/L. The results obtained show that the proposed model has excellent BG monitoring performance with a root-mean-square error (RMSE) of 1.49 mmol/L, mean absolute relative difference (MARD) of 13.42%, and Zone A + B of 99.49% in tenfold cross-validation. Therefore, we conclude that the proposed

fusion approach for BG monitoring has potentials in practical applications of diabetes management.

**Index Terms**—Electrocardiogram (ECG), feature fusion, multimodal fusion, noninvasive blood glucose (BG) monitoring, photoplethysmogram (PPG).

## I. INTRODUCTION

**D**IABETES, which results from the defects in insulin secretion, insulin action, or both, is a serious threat to global health [1]. It was estimated that the global diabetes prevalence of adults between the ages of 20 and 79 years has increased from 463 million in 2019 to 537 million in 2021 [2]. Diabetes and its complications, if not well managed, often lead to frequent hospital admissions, reduced quality of life, and undue stress on families and the society. Thus, the future global impacts of diabetes cannot be underemphasized [3]. Until now, diabetes cannot be cured. According to the international consensus of diabetes management, patients with diabetes are suggested to monitor their blood glucose (BG) regularly. Measures must be taken to maintain their BG level in a healthy range [4]. Therefore, monitoring BG at different time points is an essential part of diabetes management.

The conventional methods used for BG monitoring are finger-prick measurement and continuous glucose monitoring (CGM) device [5], [6]. However, finger-prick measurement is painful, uncomfortable, and high cost. Furthermore, this approach cannot provide a continuous way of monitoring BG levels. The probe of CGM device needs to insert into subcutaneous tissue to assess BG levels. In addition, the probe needs to be usually replaced every 7–14 days owing to the limitation of service life. Frequent replacement of CGM probe causes discomfort and pain in addition to high socioeconomic burdens, which reduces adoption and compliance of patients. Therefore, the development of an affordable and noninvasive BG monitoring approach in diabetes management is urgent and important [7].

Thus far, several noninvasive methods based on different techniques, such as optics, radio frequency, and energy metabolism, have been developed for BG monitoring [8], [9], [10], [11]. Considering that the change of BG level stimulates autonomic nervous system leading to variation in electrocardiogram (ECG) and photoplethysmogram

Manuscript received 19 August 2022; revised 1 March 2023 and 10 April 2023; accepted 17 May 2023. Date of publication 8 June 2023; date of current version 8 October 2024. This work was supported in part by the National Key R&D Program of China under Grant 2022YFB3203702, in part by the National Natural Science Foundation of China under Grant 62173318, in part by the Science and Technology Service Network Initiative (STS)-Huangpu Project under Grant STS-HP-202203, and in part by the CAS Key Laboratory of Health Informatics. (Corresponding author: Zedong Nie.)

This work involved human subjects or animals in its research. Approval of all ethical and experimental procedures and protocols was granted by the Shenzhen Institute of Advanced Technology (SIAT), Chinese Academy of Sciences Institutional Review Board under Application No. SIAT-IRB-200315-H0461, and performed in line with the Declaration of Helsinki.

Jingzhen Li, Olatunji Mumini Omisore, Yuhang Liu, Huajie Tang, Pengfei Ao, Yan Yan, Lei Wang, and Zedong Nie are with the Shenzhen Institute of Advanced Technology, Chinese Academy of Sciences, Shenzhen 518055, China (e-mail: lijz@siat.ac.cn; omisore@siat.ac.cn; yh.liu2@siat.ac.cn; hj.tang@siat.ac.cn; pf.ao@siat.ac.cn; yan.yan@siat.ac.cn; wang.lei@siat.ac.cn; zd.nie@siat.ac.cn).

Jingjing Ma is with the Testing and Technology Center for Industrial Products of Shenzhen Customs, Shenzhen 518067, China (e-mail: jingjing-0816@sohu.com).

Digital Object Identifier 10.1109/TNNLS.2023.3279383

(PPG), the ECG and PPG signals can be used to achieve BG monitoring [12], [13]. In comparison with other noninvasive methods, ECG and PPG signals are easy to obtain with wearable devices. This provides a cost-effective and comfortable solution for patients with diabetes [14], [15]. The applications of ECG and PPG for BG monitoring have been an active research topic in recent years. In [16], four different features, namely, the heart rate (HR), QTc, change of HR, and change of QTc, were extracted from ECG signal, and an extreme learning machine algorithm was developed for hypoglycemia monitoring. In [17], ECG features, such as QTc and RT-amplitude ratio, were extracted and principal component analysis algorithm was suggested for monitoring hypoglycemic events. In [18], Gaussian fitting was employed for PPG feature extraction. Specifically, the half-width and peak amplitude of the modeled Gaussian curves were used as the PPG features. Additionally, three different machine learning algorithms were used to realize three BG ranges monitoring. With the development of artificial intelligence, deep learning methods have been adopted for automatically extracting different discriminative features from physiological signals [19], [20]. In [21], the convolution neural networks—long short-term memory networks (CNN-LSTM) models were presented to achieve feature extraction and nocturnal hypoglycemia monitoring. Similarly, the ECG features were automatically obtained by autoencoder technique, and then, the convolution neural networks (CNN) were used to achieve the monitoring of nocturnal hypoglycemia in [22]. In our previous studies, an approach of DBSCAN-CNN was developed to achieve ECG feature extraction and three BG ranges monitoring [23].

Recently, multimodal fusion has gained popularity in several areas by fusing two or more data modalities to achieve better results [24], [25], [26], [27]. Some researchers have explored coupling multiple data modalities for BG monitoring. In [28], four PPG signals at different wavelengths were acquired, and the two regression algorithms were employed to improve the accuracy of BG monitoring. The photoacoustic spectroscopy and broadband dielectric spectroscopy were obtained from glucose aqueous solution in [29]. Furthermore, the relation between spectroscopy intensity and glucose concentration was studied by partial least square. In [30], a fusion method that combined impedance spectroscopy and multiwavelength spectroscopy was proposed for BG estimation.

In summary, there is a large amount of studies about the feature extraction of ECG and PPG. However, there are several limitations in the previous studies. First, most studies extracted the morphological or temporal features directly from original ECG or PPG signal, and those features were used to develop systems for BG monitoring. However, many researchers have proved that the changes of ECG and PPG are nonstationary and nonlinear owing to the fact that they may be affected by emotion, health status, and so on. A simple feature analysis is unable to extract all the information contained in these signals [31], [32]. Thus, a further investigation on feature extraction of physiological signals from spatiotemporal perspective is essential [33], [34]. Second, the previous studies mainly concentrated on individual ECG or PPG modality.

Uneven changes in the physiological signals related to BG levels have high individual differences owing to the different responses of BG homeostasis among individuals [22]. In the case of individual differences, the accuracy of BG monitoring based on individual modality is usually low. While many studies have focused on the general areas of multiple modalities, only little work specifically deals with using multimodal ECG and PPG signals for BG monitoring. Furthermore, those researches mainly concentrated on the decision level fusion by using small dataset. Taking into account that the contributions of ECG and PPG features on BG monitoring are different, a further study on multilevel feature fusion and multimodel decision fusion based on a larger dataset is important. Third, it is noteworthy to stress that the above studies mainly focused on BG ranges (i.e., hyperglycemia or hypoglycemia) rather than BG value measurement. However, the monitoring of BG ranges only reflects the risk of hyperglycemia or hypoglycemia. For diabetes management, it cannot yield whole-day information about glycemic variability that may be associated with diabetes complications [35].

This study aimed to develop a multimodal signal fusion framework for noninvasive and real-time BG monitoring. The framework performs extraction and fusion of spatiotemporal ECG and PPG features and applies weight-based Choquet integral multimodel approach. The main novelties and contributions of our article are described as follows.

- 1) For the extraction of multiple dimension features, numerical analysis and residual networks (ResNets) are designed for extracting temporal statistical and spatial morphological features from ECG and PPG signals, respectively.
- 2) To focus on suitable features and reduce computational complexity of the BG monitoring model, the extracted 160 temporal statistical features are analyzed using univariate feature selection (UFS), recursive feature elimination (RFE), and L1-based feature selection (L1-FS) techniques. Intersections of three feature selection methods are selected and used for the actual BG monitoring.
- 3) A weight-based Choquet integral multimodel approach is proposed for fusing the extracted spatiotemporal features to achieve BG monitoring.

In addition, a larger ECG-PPG-BG dataset was created through 103-day signal acquisition in 21 participants. The dataset was used for validating the robustness of the proposed model, which shows an excellent BG monitoring performance with root-mean-square error (RMSE) of 1.49 mmol/L and mean absolute relative difference (MARD) of 13.42%.

The rest of this article is organized as follows. The details of the proposed spatiotemporal ECG and PPG features fusion and weight-based Choquet integral multimodel approach are presented in Section II. Section III is about the experimental setup and data acquisition, while the experimental results and discussion are reported in Sections IV and V, respectively. Finally, the conclusions from this study are presented in Section VI.

## II. PROPOSED METHODOLOGY

### A. Algorithm Framework

Using the idea of information fusion, we proposed a multilevel feature fusion and weight-based multimodel approach for BG monitoring based on ECG and PPG signals. The code of our model is available (<https://github.com/SIATCAS/SFF-WCIM>). The proposed methodology, consisting of three different fusion levels, is presented in Fig. 1. The details of each level in the BG monitoring framework are given as follows.

*Level 1:* The ECG and PPG signals, measured with different sensors, were collected and fused into pools used for data division. Considering the influence of motion artifacts and other noises, a finite impulse response low-pass filter with a cutoff frequency of 40 Hz and a high-pass filter with a cutoff frequency of 0.5 Hz were adopted to remove baseline wander, power line interference, and motion artifact noise [36], [37], [38]. The ECG length used for BG monitoring was a window of 20 consecutive cardiac cycles in this article. It was approximately 16 s when the HR was 75 bpm. The BG values were measured every 5 min automatically by CGM system. The signal segment of 20 consecutive cardiac cycles was paired with the nearest BG value. For example, the BG values were measured at 9:30, 9:35, 9:40, and so on. The signal segments that acquired during the time of 9:30–9:34 would be correspond with the BG value measured at 9:30. On this basis, the window of 20 consecutive cardiac cycles was split into 20 individual segments, and each segment was a complete ECG waveform at a cardiac cycle. The PPG data were preprocessed in a similar way to the ECG data.

*Level 2:* The strategy of spatiotemporal feature fusion was designed with the following five basic steps.

- 1) *Cardiac Cycles Decomposition and Reconstruction:* The ECG and PPG signals with the length of 20 consecutive cardiac cycles were subjected to discrete wavelet transform (DWT) to decompose up to seven levels. Then, to extract features from different dimensions, the signals were reconstructed at various detailed coefficient levels of the DWT.
- 2) *Temporal Statistical Feature Extraction:* The ECG and PPG signals were processed to extract the temporal statistical features through numerical analysis, respectively. Specifically, probability distributions of kurtosis and skewness and information complexity, like signal mobility (SM) and Shannon entropy (SE), were extracted from each reconstructed signal and original signal. There are 80 temporal statistical features extracted from ECG signals and 80 temporal statistical features extracted from PPG signals.
- 3) *Optimal Feature Selection:* To determine the contributions of different temporal statistical features and select suitable feature for BG monitoring, the candidate features were ranked by using three feature selection methods, i.e., UFS, RFE, and L1-FS. The features are deemed suitable when ranked in top-80 with the Pearson's correlation  $|r| > 0$ ,  $p\text{-value} < 0.05$  in each feature selection method.

4) *Spatial Morphological Feature Extraction and Compression:* Morphological details were extracted from 20 individual segments of ECG and PPG signals, respectively, by the five-layer ResNets. There were 33 280 ECG features and 33 280 PPG features acquired from ResNets automatically. In addition, deep neural networks (DNNs), which consisted of multiple hidden layers, was presented to achieve feature compression. Finally, a total of 40 spatial morphological features were obtained by DNN model.

5) *Spatiotemporal Feature Combination:* A linear combination technique was performed to fuse extracted temporal statistical features and spatial morphological features to build a feature fusion matrix, which can be represented as  $F_{\text{fusion}} = \{F_{\text{temporal}}, F_{\text{morphological}}\}$ .

*Level 3:* A multimodel fusion strategy based on weight-based Choquet integral was adopted in this level. This fusion strategy has the following three basic steps.

- 1) *BG Monitoring Algorithms:* Three classical machine learning algorithms, namely, random forest, gradient boost, and bagging, were employed for preliminary BG monitoring when the temporal statistical features matrix, spatial morphological features matrix, and feature fusion matrix were used as an input, respectively. Thus, a total of  $3 \times 3 = 9$  results could be obtained, and those results were referred to as “different models” in this article.
- 2) *Choquet Integral:* Considering that the above models cannot be a cap-fits-all model especially for different individuals, the Choquet integral approach was designed for BG monitoring based on the BG historical prediction values and BG current prediction value.
- 3) *Weight-Based Multimodel Fusion:* According to the BG prediction error of each model, the weights of different models were adaptive. Combined with the weight value of each model, the final result of fusing nine models would be obtained. Hence, using multimodel fusion is expected to provide a high accuracy for BG monitoring.

### B. Temporal Statistical Feature Extraction and Feature Selection

In recent published work, the features were simply extracted from original signal for BG monitoring. In this article, we propose a new approach using spatiotemporal features to solve the problem. As described in Fig. 2, specifically, the temporal statistical features and spatial morphological features were obtained from ECG and PPG signals and then combined together. In this section, we will introduce the method of temporal statistical feature extraction, which includes data preprocessing based on DWT, feature calculation, and feature selection.

1) *Data Preprocessing Based on DWT:* The DWT is an effective signal analysis tool, which can transform the signal from time domain to wavelet domain and deliver different coefficient values. As described in Fig. 3, the first level of decomposition can be achieved if a given original ECG signal is convoluted with a high-pass filter and a low-pass filter, respectively. Once filtering is done, the low coefficient (i.e.,

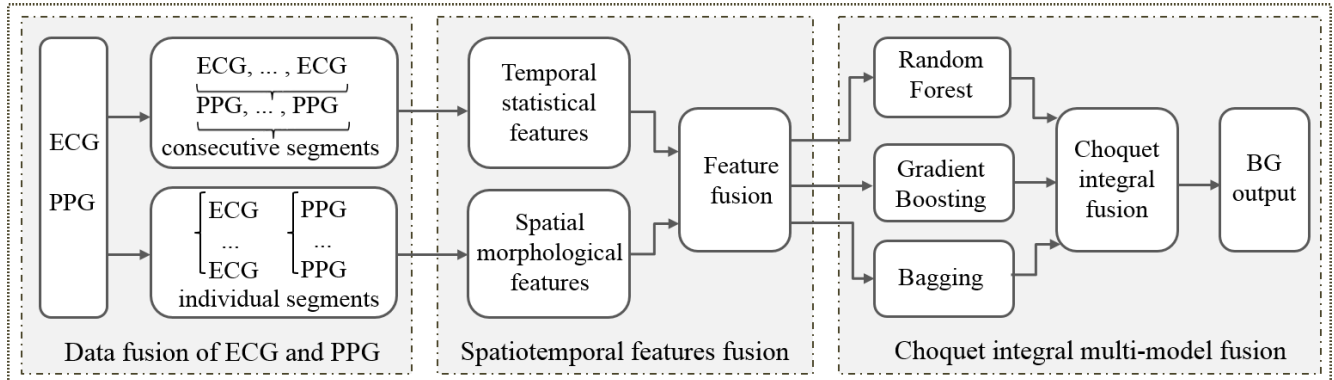


Fig. 1. Algorithm framework of BG monitoring based on ECG and PPG signals.

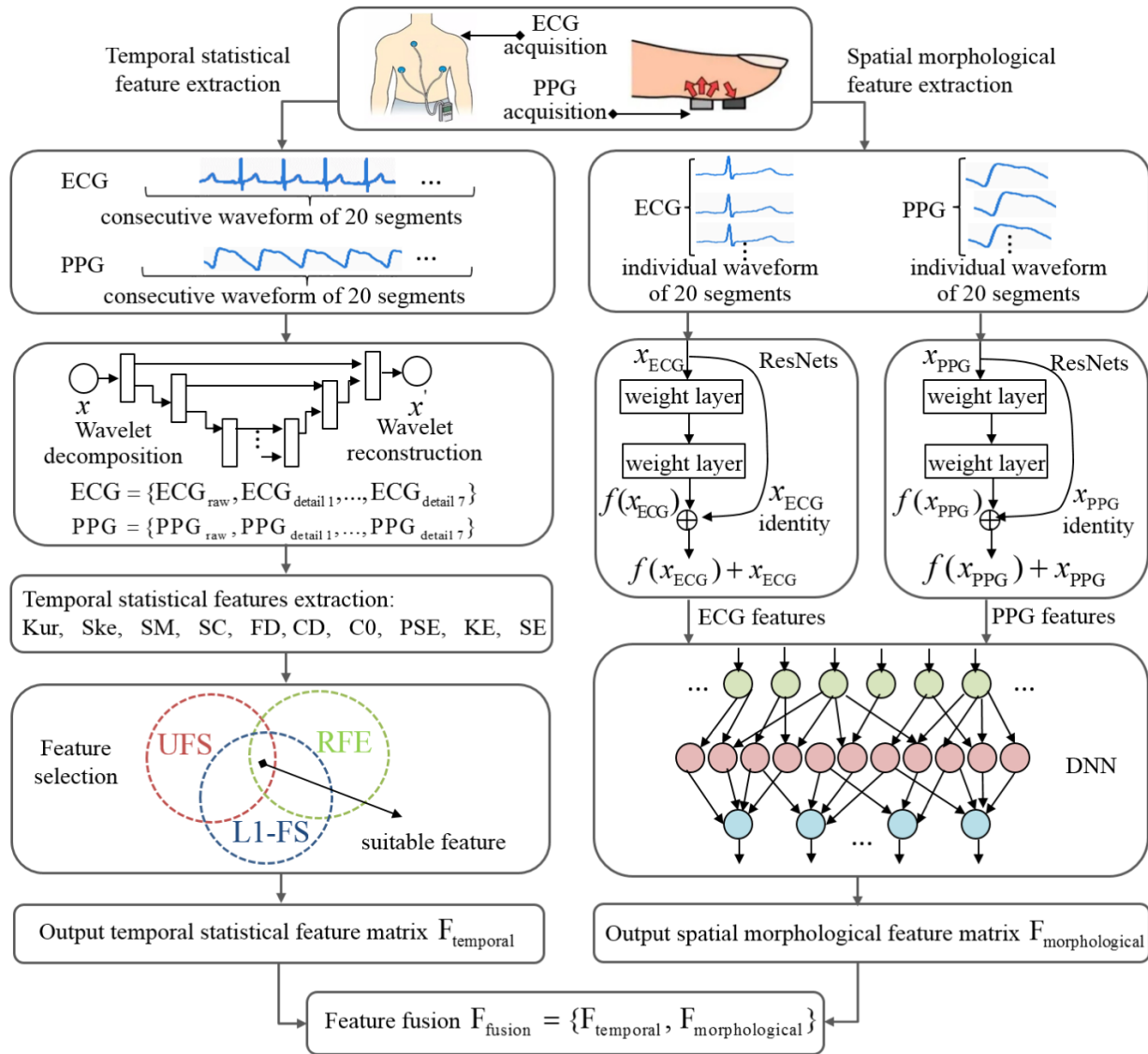


Fig. 2. Flowchart of the proposed spatiotemporal ECG and PPG features fusion.

cA1) that reflects the approximate features and the high coefficient (i.e., cD1), which characterizes the detailed features, would be obtained, as listed in (1). In the second level of decomposition, the low coefficient (i.e., cA1) was subjected

to the low-pass filter and high-pass filter again, and then, the low coefficient of cA2 and high coefficient of cD2 would be obtained. This procedure is repeated for different levels of decomposition. In this article, we used db4 as mother wavelet

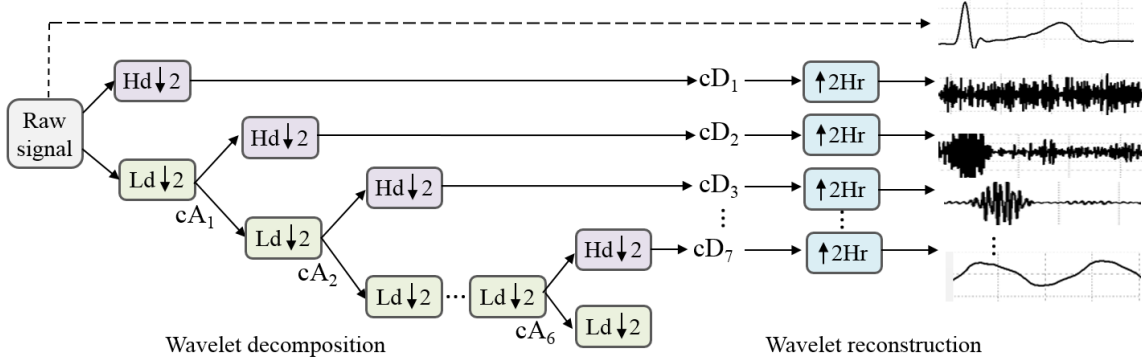


Fig. 3. Flowchart of DWT decomposition and reconstruction on ECG and PPG signals at different levels.

function, and we carried out DWT on ECG signal up to seven levels

$$\begin{cases} cA_1[n] = \sum_{k=0}^{K-1} x[2n - k]g[k] \\ cD_1[n] = \sum_{k=0}^{K-1} x[2n - k]h[k]. \end{cases} \quad (1)$$

In order to extract ECG temporal statistical features from different dimensions, we performed DWT reconstruction using different detailed coefficients from  $cD_1$  to  $cD_7$ . Thus, seven reconstructed ECG signals and the original ECG signal were stored in the signal sequence database. The PPG signal was preprocessed in a similar way to ECG signal.

2) *Temporal Statistical Feature Extraction*: The temporal statistical features, including the linear features of kurtosis (Kur) and skewness (Ske), and the nonlinear features of SM, signal complexity (SC), fractal dimension (FD), correlation dimension (CD), C0-complexity (C0), power spectral entropy (PSE), Kolmogorov entropy (KE), and SE were extracted from the original signal and DWT reconstruction signals at various detailed coefficient levels.

3) *Feature Selection*: In terms of the proposed method in above section, the temporal statistical features of ECG and PPG signals were extracted, respectively. The feature matrices of ECG and PPG signals are shown as follows:

$$F_{ECG\_temporal} = \{F_{E0}, F_{E1}, F_{E2}, F_{E3}, F_{E4}, F_{E5}, F_{E6}, F_{E7}\} \quad (2)$$

$$F_{PPG\_temporal} = \{F_{P0}, F_{P1}, F_{P2}, F_{P3}, F_{P4}, F_{P5}, F_{P6}, F_{P7}\} \quad (3)$$

where  $F_{E0}$  is the feature of original ECG signal, and  $F_{Ei}$  is the feature of DWT reconstruction signals at different detailed coefficient levels, and  $i$  is from 1 to 7. In addition, there are ten features in  $F_{Ei}$ . Specifically,  $F_{Ei}$  can be expressed as  $F_{Ei} = \{Kur_{Ei}, Ske_{Ei}, SM_{Ei}, SC_{Ei}, FD_{Ei}, CD_{Ei}, C0_{Ei}, PSE_{Ei}, KE_{Ei}, SE_{Ei}\}$ . The explanation of PPG features in (3) is similar to the ECG features.

A linear combination technique was used to fuse ECG features and PPG features. The new feature matrix  $F_{temporal\_all} = \{F_{ECG\_temporal}, F_{PPG\_temporal}\}$ , which consisted of 160 features, was built. However, on the other hand, whether these features are related to BG changes and how strong are the correlations is unknown. In order to determine the contributions of the different features and find the suitable features from feature

matrix  $F_{temporal\_all}$ , the feature selection discussed earlier was implemented. Also, this was done to eliminate redundant features and reduce processing time. According to the different combinations of feature evaluation function and regression model, the feature selection methods can be divided into three categories: filter, wrapper, and embedding. To achieve feature selection from different perspectives, as demonstrated in the following sections, three feature selection methods, namely, UFS, RFE, and L1-FS, were considered and taken as an example in this study. The candidate features of feature matrix  $F_{temporal\_all}$  will be considered as the suitable features if the candidate features satisfy two conditions.

- 1) Ranked in the top 80 in each feature selection method, and the Pearson's correlation  $|r| > 0$  and  $p\text{-value} < 0.05$ .
- 2) Selected by three feature selection methods simultaneously. In other words, the suitable features were the intersection of three feature selection methods.

The reasons why the above two conditions were used for selecting suitable feature are as follows. First, as revealed in previous studies on artificial and natural datasets, feature selection method typically eliminated well over half the features. In most cases, classification accuracy using the reduced feature set equaled or bettered accuracy using the complete feature set [39]. Hence, the top 80 out of 160 features are selected in this article. Meanwhile, to make sure that selected features are significantly correlated with BG changes, the correlation  $|r|$  should be greater than 0 and  $p\text{-value}$  should be lower than 0.05. Second, the features should be selected by different feature selection techniques simultaneously in this article. The purpose of considering multiple feature selecting is to validate that if a technique selects a feature, another technique should identify a similar feature, which is beneficial to improve the robustness of features.

a) *Univariate feature selection*: The UFS is an approach that works by selecting the best features based on univariate statistical tests. It can estimate the degree of linear dependency between two random variables. This is done in two steps. In the first step, the cross correlation between each variable and the target is computed, which is given as follows:

$$I(X_i; Y) = \frac{(X[:, i] - \text{mean}(X[:, i])) \cdot (Y - \text{mean}(Y))}{\text{std}(X[:, i]) \cdot \text{std}(Y)} \quad (4)$$

where  $X[:, i]$  is the temporal statistical features of ECG and PPG signals,  $\text{mean}(X[:, i])$  and  $\text{std}(X[:, i])$  are the mean value and standard deviation of features at the  $i$  column, respectively, and  $\text{mean}(Y)$  and  $\text{std}(Y)$  are the mean value and standard deviation of BG values, respectively. In the second step, the result obtained from (4) is converted to  $F$  score and then to a  $p$ -value. According to the  $p$ -values ( $p$ -values should be lower than 0.05), the suitable features would be selected.

*b) Recursive feature elimination:* The RFE is a popular wrapper-type feature selection algorithm. The main idea of this algorithm is to select features by recursively considering smaller and smaller sets of features based on an external estimator that assigns weights to features. The external estimator was set as random forest classifier in this study. The feature selection process is as follows. First, the estimator of random forest classifier is trained on the initial set of features, and the importance of each feature is obtained in terms of the training result. Since a forest averages the predictions of a set of  $m$  trees with individual weight functions  $W_j$ , the predictions of random forest classifier can be expressed as (5). Second, according to the importance of each feature, the least important features are pruned from current set of features. That procedure is recursively repeated on the pruned set and the important features are preserved

$$\hat{y} = \frac{1}{m} \sum_{j=1}^m \sum_{i=1}^n W_j(x_i, x') y_i = \sum_{i=1}^n \left( \frac{1}{m} \sum_{j=1}^m W_j(x_i, x') \right) y_i. \quad (5)$$

*c) L1-based feature selection:* Considering that the linear models penalized with the L1 norm have sparse solutions, many of their estimated coefficients are zero. Therefore, when our goal is to reduce the dimensionality of the data, we can use L1 norm along with SelectFromModel to select the nonzero coefficients. Specifically, SelectFromModel is a metatransformer that can be used alongside different estimators. It can assign importance to each feature through a specific attribute after fitting. In this article, the sparse estimator used for this purpose is the Lasso for regression. The optimization objective of Lasso is listed as follows:

$$J_\beta(\beta) = \frac{1}{N} \sum_{i=1}^N (Y_i - \hat{Y}_i)^2 + \lambda \sum_{j=1}^p |\hat{\beta}_j| \quad (6)$$

where  $|\hat{\beta}_j|$  is the L1 norm, and  $\lambda \sum_{j=1}^p |\hat{\beta}_j|$  is the shrinkage penalty used to reduce the number of features.

### C. Spatial Morphological Feature Extraction and Compression

The details of the spatial morphological feature extraction from ECG and PPG signals and modality for fusion are given here. The algorithm includes two modules: a five-layer ResNets and a three-hidden-layer DNN. The training process of algorithm is as follows. First, the morphological features were extracted by means of ResNet. Then, the output of ResNet (i.e., morphological features) was adopted as the input of DNN to realize the feature compression. Third, the objective function was calculated by comparing the difference

between label information (i.e., BG reference value provided by Dexcom G6) and BG prediction value in the model. Finally, the connection weight and bias of hidden layers of ResNet and DNN are automatically adjusted by the system.

*1) Spatial Morphological Feature Extraction:* Recently, CNN has led to a series of breakthroughs for feature extraction owing to its powerful learning ability. The evidence reveals that the network depth of CNN is of crucial importance because of features can be enriched by the number of stacked layers (depth). However, on the other hand, with the increase of network depth, the network exists the problem of vanishing/exploding gradients. In this article, in order to extract richer features and avoid vanishing/exploding gradients, as demonstrated in Fig. 4, the five-layer ResNets, which is a novel type of CNN, were proposed in this article. ResNets utilize skip connections or shortcuts to jump over some layers. It is consisted of one convolution block and multiple identity blocks in different layers. In particular, the convolution block, which has convolution operation in jump connection, is used to change the network dimension. The identity block, which uses shortcuts to jump connection, is used to change the network depth. The process of convolution block is listed as follows:

$$y_{\text{conv\_block}} = \text{ReLU} \left[ \text{BatchNorm} \left( f_{i,j}^{(l)}(x) \right) + \text{BatchNorm} \left( f'_{i,j}^{(l)}(x) \right) \right] \quad (7)$$

where  $f_{i,j}^{(l)} = \sum_{p=1}^s \sum_{q=1}^s \chi_{i+p-1,j+q-1}^{(l-1)} \cdot k_{p,q}^{(l)} + b^{(l)}$  is the convolution operation when the input feature map of  $l-1$  layer is  $\chi^{(l-1)}$ , and the convolution kernel is  $k^{(l)}$ . In addition,  $f'_{i,j}^{(l)}(x)$  represents the three convolution operations.  $\text{BatchNorm}(f_{i,j}^{(l)}(x))$  and  $\text{BatchNorm}(f'_{i,j}^{(l)}(x))$  are the batch normalization operation. The output would obey the normal distribution after batch normalization, as shown in the following:

$$\begin{cases} \mu_\beta \leftarrow \frac{1}{m} \sum_{i=1}^m z^{(l)} \\ \sigma_\beta^2 \leftarrow \frac{1}{m} \sum_{i=1}^m (z^{(l)} - \mu_\beta)^2 \\ \hat{z}^{(l)} \leftarrow \frac{z^{(l)} - \mu_\beta}{\sqrt{\sigma_\beta^2 + \varepsilon}} \\ y^{(l)} \leftarrow \gamma \hat{z}^{(l)} + \psi \end{cases} \quad (8)$$

where  $z^{(l)}$  is the output result of convolution operation. ReLU, which is a noncontinuous activation function, is defined as (9). The output is represented in (10) after the activation function

$$\xi(y) = \begin{cases} 0, & y \leq 0 \\ y, & y > 0 \end{cases} \quad (9)$$

$$a^{(l)} = \xi(y^{(l)}). \quad (10)$$

Taking into account that the identity block uses shortcuts to jump connection, the process of identity block can be expressed as follows:

$$y_{\text{identity\_block}} = \text{ReLU} \left[ x + \text{BatchNorm} \left( f'_{i,j}^{(l)}(x) \right) \right]. \quad (11)$$

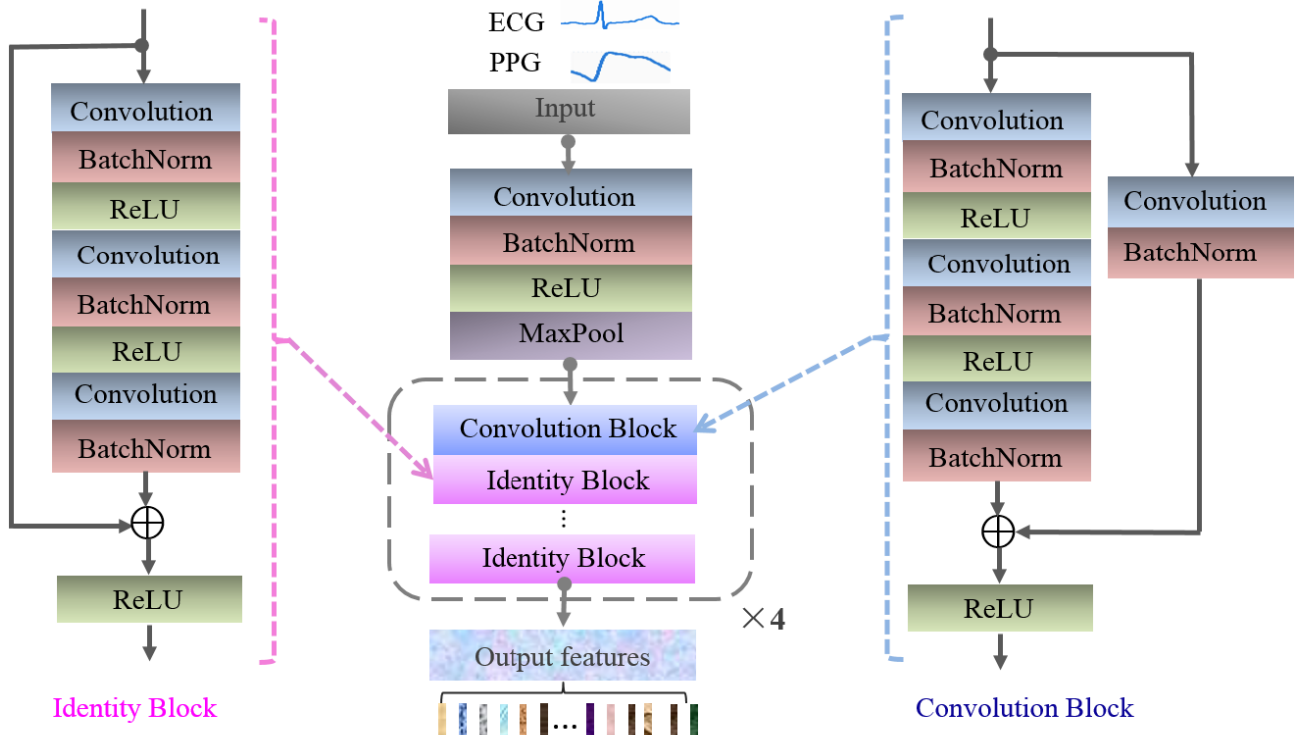


Fig. 4. Algorithm structure of ResNets using for spatial morphological features extraction of ECG and PPG signals.

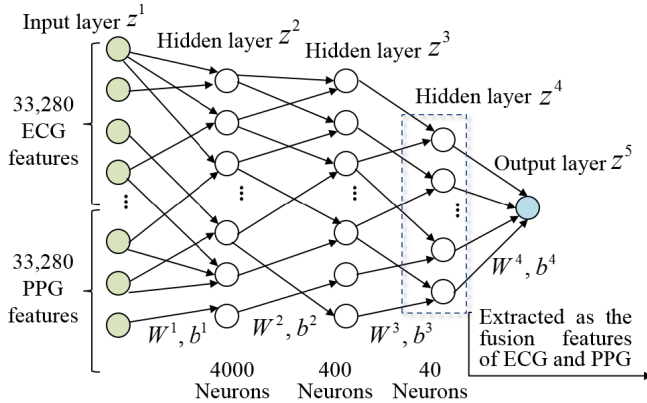


Fig. 5. Algorithm structure of DNN using for spatial morphological features compression and fusion of ECG and PPG signals.

According to the relevant references and our previous studies [40], [41], the configuration details and hyperparameters of the proposed ResNets are as follows. The numbers of convolution kernel were 4, and the convolution kernel size was  $1 \times 6$  in the first layer. In addition, the max-pooling size was set as  $1 \times 2$ . The remaining each layer was composed of one convolution block and multiple identity blocks. Specifically, the numbers of identity blocks were 2, 3, 5, and 2, respectively. The convolution kernel size of convolution block was  $1 \times 6$ , and the convolution kernel size of identity block was  $1 \times 5$ . The numbers of convolution kernel were 16 in the second layer, 32 in the third layer, 64 in the fourth layer, and 128 in the fifth layer.

**2) Spatial Morphological Feature Compression and Fusion:** The number of extracted features depends on the number of convolution kernel and convolution kernel size in ResNet. According to the hyperparameter setting in ResNet, a total of 33 280 ECG spatial morphological features and 33 280 PPG spatial morphological features were obtained. As described in Fig. 5, to achieve feature compression and fusion of ECG and PPG features, the DNN was presented in our work. The DNN includes an input and an output layer and three hidden layers. The numbers of neurons were 4000, 400, and 40 in the hidden layers, respectively. In addition, to reduce overfitting, there is a dropout layer between two adjacent hidden layers. The dropout ratios were set as 0.3 and 0.2, respectively. The data in the third hidden layer were hooked from DNN and considered as the features of ECG and PPG after compression. The output layer of DNN is the prediction value of BG. The process of feature compression and fusion is as follows. Assuming that the variable of  $l$  layer is  $z^l$ , the output of  $l + 1$  layer can be expressed as follows:

$$\begin{cases} a^{l+1} = W^l z^l + b^l \\ z^{l+1} = \Psi^{l+1}(a^{l+1}) \end{cases} \quad (12)$$

where  $b^l$  is the bias term of output, and  $W^l$  is the weight value. Weights and bias are both learnable parameters inside the network and they can be obtained and optimized by the DNN automatically. First, the DNN will randomize both the weight and bias values before learning initially begins. As training continues, both parameters are adjusted toward the desired values and the correct output.

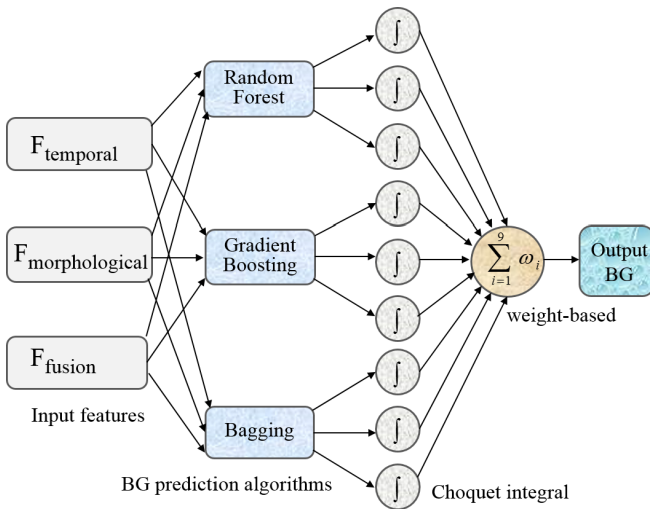


Fig. 6. Algorithm structure of decision fusion using weight-based Choquet integral multimodel approach.

#### D. Decision Fusion Using Weight-Based Choquet Integral Multimodel Approach

In order to improve the accuracy of BG monitoring, the decision fusion based on weight-based Choquet integral multimodel approach was proposed in this section. As illustrated in Fig. 6, the fusion approach operates in three main stages by carrying the following processes.

In the first stage, considering that the algorithms of random forest, gradient boost, and bagging can achieve a relatively high accuracy of BG monitoring in our study, the above three algorithms were adopted to achieve the BG monitoring in this article when the features of  $F_{\text{temporal}}$ ,  $F_{\text{morphological}}$ , and  $F_{\text{fusion}} = \{F_{\text{temporal}}, F_{\text{morphological}}\}$  were used as the input of algorithm, respectively. Those prediction results were referred to as “different models” in this article. Therefore, a total of  $3 \times 3 = 9$  models could be obtained in this stage.

In the second stage, the BG value of each model was fused, respectively, based on the BG historical prediction values and BG current prediction value by using Choquet integral. It is necessary to introduce fuzzy measure before introducing Choquet integral. In particular, assuming that  $X = \{x_1, x_2, \dots, x_N\}$  is  $N$  sources of data/information, the fuzzy measure  $g : 2^X \rightarrow \mathbb{R}^+$  is a function which should be satisfied the following two properties of boundary condition and monotonicity: 1)  $g(\emptyset) = 0$  and 2) if  $A, B \subseteq X$  and  $A \subseteq B$ , then  $g(A) \leq g(B)$  [42]. The Choquet integral of observation  $h$  on  $X$  is expressed as (13), where  $A_{\pi(j)} = \{x_{\pi(1)}, x_{\pi(2)}, \dots, x_{\pi(j)}\}$ ,  $g(A_{\pi(0)}) = 0$ , and permutation  $\pi$ , such that  $h_{\pi(1)} \geq h_{\pi(2)} \geq \dots \geq h_{\pi(N)}$ . With guided trial-and-error approach,  $N$  was set as 7, indicating that six closest BG historical values and the current value were used for analysis in each model

$$\int h \circ g = C_g(h) = \sum_{j=1}^N h_{\pi(j)}(g(A_{\pi(j)})) - g(A_{\pi(j-1)}). \quad (13)$$

In the third stage, the weight-based was adopted to fuse the prediction result of each model after Choquet integral. The

weight of the  $i$ th model could be defined as of (14), where  $R_k = 1/((\sum_{t=1}^T (r_t - r'_t)^2)/T)^2$ ,  $r_t$  and  $r'_t$  are the prediction value and reference value of training dataset, and  $T$  is the number of BG values in the training dataset. Hence, the weight of each model was adaptive. The BG output of fusing nine models can be represented as (15), where  $r''_k$  is the output of each model after Choquet integral in the testing dataset

$$\omega_i = \frac{R_i}{\sum_{k=1}^9 R_k} \quad (14)$$

$$BG_{\text{fusion}} = \sum_{k=1}^9 \omega_k \cdot r''_k. \quad (15)$$

#### E. Assessment Metrics

To quantify the BG prediction performance of the proposed fusion approach, the following metrics, namely, RMSE, MARD, and Parkes error grid between the prediction values and reference values serve as the primary indicators to evaluate the accuracy. The definitions of RMSE and MARD are given in the following:

$$RMSE = \sqrt{\frac{1}{N} \sum_{j=1}^N (y(j) - y'(j))^2} \quad (16)$$

$$MARD = \frac{1}{N} \sum_{j=1}^N \left| \frac{y(j) - y'(j)}{y(j)} \right|. \quad (17)$$

RMSE and MARD can provide an overall indication of BG prediction performance. RMSE is a measure of BG prediction errors for different models owing to its scale-dependent [43]. MARD is the average of the absolute error between BG prediction values and BG reference values. A small percentage indicates that the prediction values are close to reference values [44].

Parkes error grid analysis, which is also known as consensus error grid analysis, is developed as a new tool for evaluating performance zones for BG monitoring [45]. It is divided into five different zones called zones A–E. Each zone represents a degree of risk of an adverse outcome due to the error in predicted BG values. A larger percentage in zones A and B (especially in zone A) means better prediction performance.

### III. EXPERIMENTAL SETUP

#### A. Study Participant

In this article, 21 adults, including 17 normal individuals and four diabetic individuals, were recruited from the Shenzhen Institute of Advanced Technology, Chinese Academy of Sciences (SIAT-CAS) between August 2020 and July 2021. Those participants are characterized as 12 males and nine females, with their ages range between 20 and 63 years (mean: 36.9 years) and do not have heart-related and blood diseases. The study was approved by the ethics committee of the institute with approval number SIAT-IRB-200315-H0461. Finally, written informed consent was obtained from each participant before conducting data acquisition.

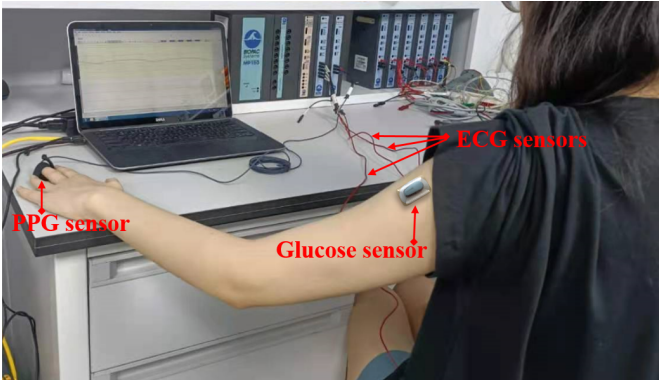


Fig. 7. Capturing the ECG and PPG signals and BG values of a participant during the experiment.

### B. Data Acquisition

To eliminate the interference of other issues, such as movement, drug, and environment as possible, the experiment was conducted under predesigned controlled conditions. Each participant was asked to fast for at least 8 h before his/her experiment and was prevented from any intense exercise or drug usage within 2 h prior to the experiment. As shown in Fig. 7, the participant was seated to put himself/herself in a relaxed state during the experiment. Three ECG sensors were attached on the sixth rib of the left anterior axillary line, the junction of the right clavicle and sternum, and the lowest rib on the right side, respectively. PPG sensor was placed on the middle finger of the left hand and fixed with a bandage. The experiment started at 9:00 am and lasted for 150 min for each participant every day. The data were collected continuously during the experiment. Specifically, BG values were measured by using commercial CGM system-Dexcom G6 (Dexcom, San Diego, CA, USA), which has been approved by Food and Drug Administration. The reading range of Dexcom G6 is within 2.2–22.2 mmol/L, and it can collect and save BG value every 5 min. ECG and PPG signals were recorded with ECG 100C and PPG 100C devices (BIOPAC, Goleta, CA, USA) with the sampling frequency of 1000 Hz. The experimental process is as follows. First, ECG and PPG signals were obtained from each participant in a fasting state, which lasted for 30 min. Subsequently, the participant was given 100-g bread and 250-mL water to ingest at 9:30. The data were collected continuously during food intake. The data collection was terminated at 11:30.

In our article, a total of 103 days of ECG and PPG signals encompassing 21 participants were collected. The range of BG levels of enrolled participants was from 2.2 to 21.8 mmol/L during the experiments (103 days). Considering that the physiological signals of each individual are different and the physiological signals at different days are also different for the same individual, the data of 103 days can reflect the changes of physiological signals for partial population to a certain extent. Table I describes the data acquisition of the study population. There were 86 days of data (986 340 heartbeats) obtained from 17 normal individuals, and 17 days of data (203 240 heartbeats) obtained from four diabetic individuals. To verify the feasibility of BG monitoring using ECG and PPG, the

TABLE I  
DATA ACQUISITION OF THE STUDY POPULATION

ID	Type	Days	The number of heartbeats for each day
01	N	5	11340 / 11600 / 11860 / 12100 / 11780
02	N	5	10480 / 9680 / 10680 / 10480 / 10240
03	N	5	13740 / 14020 / 14020 / 13020 / 13120
04	N	4	12500 / 12640 / 13080 / 12880
05	N	5	9020 / 9960 / 9640 / 10080 / 9780
06	N	5	12700 / 12980 / 12360 / 11360 / 10940
07	N	5	10300 / 13560 / 10700 / 10820 / 11060
08	N	6	11960 / 12880 / 12540 / 11320 / 11280 / 11160
09	N	5	11700 / 10200 / 11200 / 10600 / 10800
10	N	6	11960 / 11600 / 12440 / 11020 / 10720 / 11020
11	N	4	10920 / 10920 / 10740 / 11040
12	N	5	11580 / 11340 / 11300 / 10820 / 10940
13	N	6	11300 / 10120 / 10660 / 10760 / 11300 / 10720
14	N	5	11080 / 11360 / 11860 / 12980 / 11500
15	N	5	13740 / 13000 / 12580 / 12500 / 12800
16	N	5	10400 / 9800 / 10320 / 10040 / 10040
17	N	5	12460 / 11360 / 11340 / 12580 / 11220
18	D	4	11640 / 11980 / 12080 / 11980
19	D	3	9160 / 9220 / 9120
20	D	5	13800 / 13860 / 14520 / 13980 / 13600
21	D	5	13020 / 12560 / 10960 / 11260 / 10500
total		103	1189580

N: normal individual D: diabetic individual

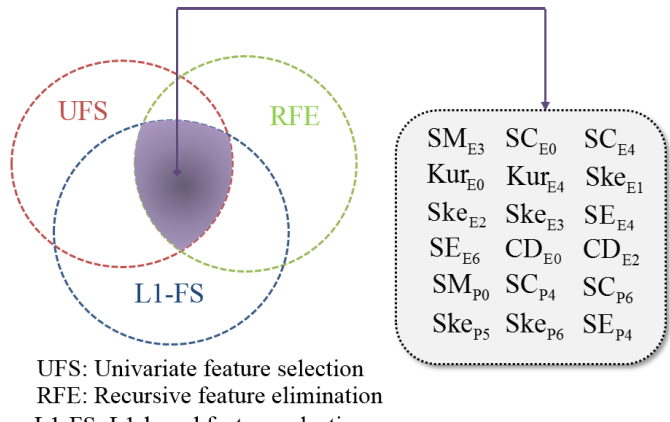


Fig. 8. Temporal features selected with the three feature selection methods.

training dataset and testing dataset were split based on days, and the tenfold cross validation method was adopted in this article. Namely, the datasets were divided into ten groups, one group (10 days) was used as the testing dataset, and the remaining nine groups (93 days) were adopted as training dataset. There were approximately 44 830 signal segments (each signal segment consisted of 20 heartbeats) of normal individuals and 8870 signal segments of diabetic individuals in training the model for each fold. The procedure was repeated ten times.

## IV. EXPERIMENTAL RESULTS

### A. Temporal Statistical Features Selection Results

Following the procedures in Section II, there were a total of 160 temporal statistical features extracted from ECG and PPG signals. We integrated the outcome of the feature selection methods to obtain consistent features that exhibit variation with the BG values. Fig. 8 describes the selected features

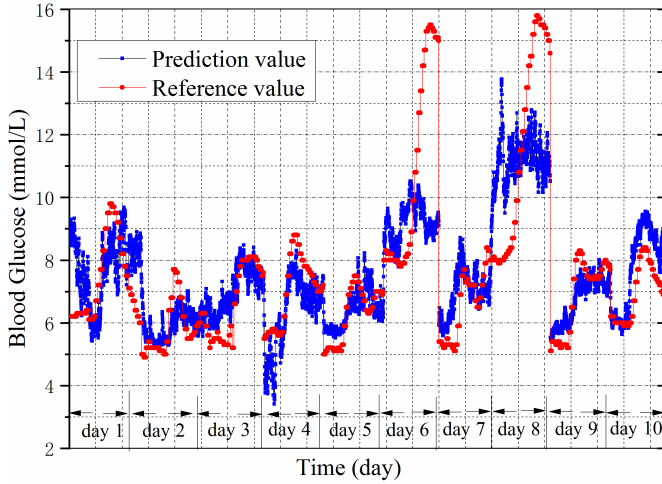


Fig. 9. Comparison of BG prediction values using the proposed fusion approach and BG reference values provided by Dexcom G6.

among the feature selection methods in tenfold cross validation. The subscripts E and P represent the features of ECG and PPG, respectively. Moreover, the subscript 0 represents that the features were extracted from the original waveform, and the subscripts from 1 to 7 represent that the features were obtained from the reconstructed signals at corresponding detailed coefficient level of DWT. Regarding the feature selection results, 12 temporal statistical features, namely,  $SM_{E3}$ ,  $SC_{E0}$ ,  $SC_{E4}$ ,  $Kur_{E0}$ ,  $Kur_{E4}$ ,  $Ske_{E1}$ ,  $Ske_{E2}$ ,  $Ske_{E3}$ ,  $SE_{E4}$ ,  $SE_{E6}$ ,  $CD_{E0}$ , and  $CD_{E2}$ , were considered as the suitable features in the ECG signal, and this was obtained upon applying the three feature selection methods. Similarly, the PPG features that were selected as suitable features were mainly focused on  $SM_{P0}$ ,  $SC_{P4}$ ,  $SC_{P6}$ ,  $Ske_{P5}$ ,  $Ske_{P6}$ , and  $SE_{P4}$ .

### B. BG Prediction Result

Fig. 9 displays the BG prediction result of 10 days in the testing dataset. With the proposed fusion approach, we observed that the BG prediction values matched the corresponding BG reference values measured from Dexcom G6. In terms of the prediction result of each day, it indicated that the BG level was low in the first 30 min owing to the participant was fasting. Furthermore, the BG levels increased gradually after participants ingested the bread, while the BG values reached their maximum values between 10:30 and 11:00. Subsequently, the BG level began to drop. Additionally, it could be observed that in comparison with days 6 and 8, the prediction values of remaining days showed a more similar trend with reference values. To prove clinical significance of the proposed fusion approach, the Parkes error grid analysis for all results of 10 days is shown in Fig. 10. It was revealed that the BG prediction value fell 100% into the clinically acceptable zones (80.48% in zone A and 19.52% in zone B). These above percentages were obtained for a total of 5663 prediction values. Therefore, the proposed approach achieved a good matching between the prediction values and reference values, providing confidence in the potential of our approach.

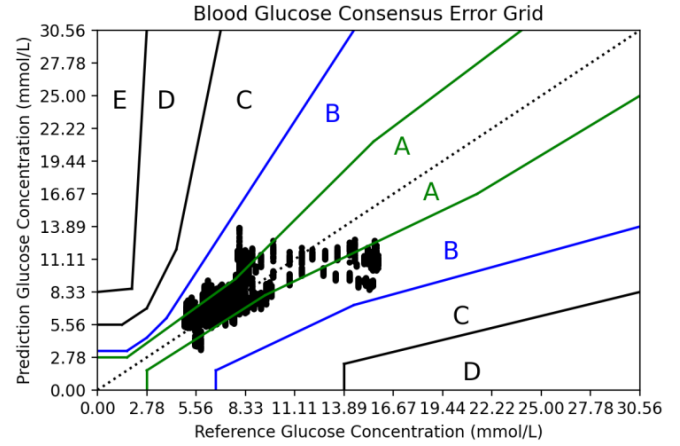


Fig. 10. Parkes error grid analysis of the proposed fusion approach.

In order to evaluate the performance of fusion technique, the tenfold cross-validation was adopted only using ECG or PPG and the fusion of ECG and PPG. Table II describes the RMSE, MARD, zone A, zone B, and zone A + B in different folds. The average RMSE, MARD, zone A, and zone A + B were 1.56 mmol/L, 13.88%, 77.90%, and 99.38% by only using ECG and were 1.82 mmol/L, 17.06%, 70.26%, and 98.53% by only using PPG.

It could be observed that the accuracy based on the fusion of ECG and PPG was significantly improved in comparison with single-modal approach. For instance, the BG prediction values of fold 1, fold 2, fold 4, fold 5, fold 7, and fold 9 fell 100% into the clinically acceptable zones. The average MARD in tenfold cross-validation was 13.42%, which was close to the typical accuracy of commercially available CGM devices (MARD: 9%–13%) has been approved by Food and Drug Administration [46], [47].

### C. Ablation Study Result

To further evaluate the performance of the proposed approach, we performed several ablation studies. The ablations were done with the machine learning algorithms listed in Table III. Each method showed different performances, and the accuracies obtained are as shown in Table IV. In method A, the RMSE, MARD, and zone A were 2.15 mmol/L, 19.15%, and 72.33%, while the temporal statistical features of ECG and PPG signals were used. The RMSE has fallen from 2.15–1.83 mmol/L and MARD has fallen from 19.15% to 14.98% in method B when the spatial morphological features of ECG and PPG signals were used. The RMSE values were 1.82 and 1.97 mmol/L and MARD values were 14.88% and 18.13% in methods C and D, respectively. In method F, the RMSE, MARD, and zone A were 1.76 mmol/L, 14.36%, and 76.95% when the weight-based multimodel fusion of random forest, gradient boost, and bagging but without Choquet integral was utilized. Method G showed the best performance with an RMSE of 1.68 mmol/L, an MARD of 13.73%, and zone A of 80.48%. Overall, this further indicates that the proposed fusion approach is effective.

TABLE II  
TENFOLD CROSS-VALIDATION PERFORMANCE OF THE PROPOSED METHOD USING DIFFERENT SIGNALS

Signal	ECG					PPG					ECG + PPG			
	Fold	RMSE (mmol/L)	MARD (%)	Zone A (%)	Zone A + B (%)	RMSE (mmol/L)	MARD (%)	Zone A (%)	Zone A + B (%)	RMSE (mmol/L)	MARD (%)	Zone A (%)	Zone A + B (%)	
1	2.04	11.54	79.61	99.93	2.81	17.26	69.75	96.65	<b>1.93</b>	<b>10.85</b>	<b>81.65</b>	<b>100</b>		
2	1.16	12.70	80.52	<b>100</b>	1.20	13.58	76.11	99.93	<b>1.10</b>	<b>12.62</b>	<b>81.69</b>	<b>100</b>		
3	1.49	17.72	77.38	95.85	1.58	19.95	73.14	95.85	<b>1.45</b>	<b>17.68</b>	<b>78.10</b>	<b>96.07</b>		
4	1.85	13.39	76.46	99.82	2.40	16.90	70.47	97.93	<b>1.83</b>	<b>12.64</b>	<b>77.84</b>	<b>100</b>		
5	1.42	14.47	72.30	<b>100</b>	1.49	13.05	73.69	<b>100</b>	<b>1.22</b>	<b>11.62</b>	<b>83.44</b>	<b>100</b>		
6	1.50	<b>13.35</b>	77.83	<b>99.91</b>	1.85	17.29	66.78	98.34	<b>1.48</b>	13.56	<b>77.85</b>	99.88		
7	<b>1.67</b>	14.35	77.19	99.95	1.74	17.91	69.13	99.89	1.68	<b>13.72</b>	<b>80.48</b>	<b>100</b>		
8	1.17	12.43	77.89	<b>99.37</b>	1.38	15.01	71.28	98.97	<b>1.13</b>	<b>12.24</b>	<b>80.40</b>	<b>99.37</b>		
9	1.98	<b>13.74</b>	<b>84.03</b>	99.27	2.13	18.59	67.61	99.20	<b>1.79</b>	<b>13.74</b>	83.25	<b>100</b>		
10	1.31	<b>15.14</b>	75.79	<b>99.70</b>	1.59	21.10	64.64	98.54	<b>1.28</b>	15.58	<b>76.27</b>	99.63		
Average		1.56	13.88	77.90	99.38	1.82	17.06	70.26	98.53	<b>1.49</b>	<b>13.42</b>	<b>80.09</b>	<b>99.49</b>	

TABLE III  
EXPERIMENTAL SETUP IN ABLATION STUDY

Method	Feature	Algorithm
A	Temporal statistical features of ECG and PPG	Random forest
B	Spatial morphological features of ECG and PPG	Random forest
C	Temporal statistical features and spatial morphological features of ECG	Random forest
D	Temporal statistical features and spatial morphological features of PPG	Random forest
E	Temporal statistical features and spatial morphological features of ECG and PPG	Random forest
F	Temporal statistical features and spatial morphological features of ECG and PPG	Weight-based multi-model fusion
G	Temporal statistical features and spatial morphological features of ECG and PPG	Weight-based Choquet integral multi-model fusion

TABLE IV  
COMPARISON OF DIFFERENT MODULES IN ABLATION STUDY

Method	RMSE (mmol/L)	MARD (%)	Zone A (%)	Zone B (%)	Zone A + B (%)
A	2.15	19.15	72.33	27.10	99.43
B	1.83	14.98	75.72	24.26	99.98
C	1.82	14.88	74.98	25.02	<b>100</b>
D	1.97	18.13	68.78	30.80	99.58
E	1.82	14.67	76.58	23.40	99.98
F	1.76	14.36	76.95	23.05	<b>100</b>
G	<b>1.68</b>	13.73	<b>80.48</b>	<b>19.52</b>	<b>100</b>

#### D. Comparison Result

The results in Table V present the prediction performance of different methods on the self-built dataset. Specifically, we selected the methods of CNN-RNN, ResNets, CDA, and CNN-MFWV for extensive comparison. Compared with these four methods, our proposed method shows the smallest RMSE of 1.49 mmol/L and the smallest MARD of 13.42%. Furthermore, the Parkes error grid analysis showed the largest zone A of 80.09%, indicating that our method could produce a high accuracy in BG monitoring.

#### V. DISCUSSION

In this article, a multilevel feature fusion approach was presented for BG monitoring. Both temporal statistical and

TABLE V  
COMPARISON RESULTS OF DIFFERENT METHODS ON THE SELF-BUILT DATASET

Ref.	Method	RMSE (mmol/L)	MARD (%)	Zone A (%)	Zone A + B (%)
[21]	CNN-RNN	1.66	14.93	75.46	99.35
[48]	ResNets	1.63	15.22	75.18	99.26
[22]	CDA	1.99	20.67	60.88	98.56
[40]	CNN-MFWV	1.61	14.71	76.96	98.94
Ours	SFF-WCIM	<b>1.49</b>	<b>13.42</b>	<b>80.09</b>	<b>99.49</b>

CNN-RNN: Convolutional neural networks and recurrent neural networks; ResNets: Residual networks; CDA: Convolutional denoising autoencoder; CNN-MFWV: Convolutional neural networks with multisegment fusion and varied-weight; SFF-WCIM: Spatiotemporal features fusion and weight-based Choquet integral multi-model

spatial morphological features of ECG and PPG signals are taken. As is known, ECG and PPG signals are easily interfered by physiological motion artifacts (e.g., movement and breath), surrounding noise, and the acquired devices (e.g., electrode and cable). Noise interference may cause waveform distortion and reduce the signal-to-noise ratio of ECG and PPG signals [49]. A simple feature analysis may not be able to extract adequate features contained in these signals for BG monitoring. Meanwhile, considering that the change of BG is approximately linear over a period and the changes of ECG and PPG signals are associated with BG level, the acquired ECG and PPG signals should carry temporal-related features. Additionally, the change of BG will trigger autonomic nervous system to maintain homeostasis (internal stability and balance) through the coordination of different organs such as heart, and it will cause the morphological change of ECG and PPG signals [50]. Based on the above reasons, we herein approached the problem by extracting both the temporal features and morphological features of ECG and PPG signals.

Recent investigations have revealed that changes of ECG and PPG signals are nonstationary, which exhibit typically complex dynamics [51]. Thus, we aimed to extract the temporal statistical features by using complex feature metrics. Namely, the features of Kur and Ske representing probability distributions and the features of SM, SC, C0, PSE, SE, and so on representing information complexity were obtained in this work. The selected features in each fold were not exactly

the same. However, the proportion of feature overlap in any twofolds was about 80%. The reason why the selected features in each fold were not the same is linked with the personalized changes of ECG/PPG and BG. Considering that individuals were not exactly the same in each fold, the selected features in each fold will not be the same. On the other hand, as shown in Fig. 8, 18 features of Kur, Ske, SM, SC, SE, and CD from the original signal and DWT reconstruction signals were considered as the suitable features in all tenfolds, indicating that those features have a strong relationship with BG changes in all enrolled individuals. Specifically, Ske and Kur are the metrics, which can reflect the histogram's deviation of normal distribution. We found that in comparison with the low BG value, the right of the center point of Ske was significant when the BG value was high. For instance, the average value of  $Ske_{E0}$  was about 1.243 when BG value was less than 5.5 mmol/L, whereas it was 1.876 when BG value was greater than 9 mmol/L. Thus, the result informs that the asymmetry of probability distribution of ECG signal would become larger if the BG is not controlled well. This may be because the function of autonomic nervous system is affected by abnormal BG level. The further analysis pointed out that other features have the similar conclusions. For example, the  $SE_{P4}$  of PPG signal was 4.02 when the BG value was 5 mmol/L, whereas the  $SE_{P4}$  was 4.10 when the BG value was 10 mmol/L. SE is an uncertainty measure for random variables. The higher the SE is, the higher the uncertainty and randomness. In this article, the result indicated that the ECG and PPG signals were tended to uncertainty owing to the SE value became greater when the BG value was out of normal range, indicating the change of BG can affect the function of autonomic nervous system. If the BG is out of normal range for a longer period, it will put unnecessary stress on the autonomic nervous system, which may lead to impaired function of cardiovascular system and the abnormal change of ECG and PPG signals.

In this article, a window of 20 consecutive cardiac cycles was adopted for BG monitoring. The reason was associated with balance between the accuracy of BG monitoring and user acceptability. First, the accuracy of BG monitoring based on single waveform at a cardiac cycle is relatively low. This can be attributed to a fact that ECG and PPG are easily interfered by noises. To avoid the impact of single poor waveform, it is necessary to use the waveforms of multiple cardiac cycles for BG monitoring. Compared with the results based on single cardiac cycle, we found that the model could achieve a high accuracy of BG monitoring when a window of 20 cardiac cycles was adopted. Second, in practical applications, the measurement time of physiological signals will affect the user acceptability. Some studies indicate that the length of 10–20 s can be acceptable to most users [52]. Therefore, the length of 20 consecutive cardiac cycles (approximately 16 s) was adopted in this article. In addition, the window of 20 consecutive cardiac cycles was divided into 20 individual segments, and those segments were used as the input of ResNets to extract the spatial morphological features of ECG and PPG signals. Each segment was a complete ECG/PPG waveform at a cardiac cycle. The reason why the size of segment was one cardiac cycle was associated with the rep-

resentation learning ability of convolution layers. Specifically, the ResNets were utilized to obtain the ECG/PPG features in our article. The ResNets are consisted of convolution blocks and identity blocks. Furthermore, the above two blocks are mainly composed of multiple convolution layers. We found that if the size of ECG/PPG segment was too large, the accuracy of BG monitoring based on ECG/PPG was low. This might be due to many duplicated features in ResNets, whereas the convolution layer is good at extracting feature from local areas [40], [53]. Thus, it was critical to choose the appropriate size of ECG/PPG segment as the input of ResNets. Considering that heart works periodically under the control of autonomic nervous system, the ECG and PPG signals, which reflect the electrical activity of heart, can be regarded as the periodic signals. Thus, the consecutive cardiac cycles were divided into 20 individual segments based on cardiac cycle.

In this article, the tenfolds of training dataset and testing dataset were obtained by splitting all data based on days, not subjects. The reason why we adopted this splitting method is associated with the personalized changes of ECG/PPG and BG. In our previous studies, we found that both physiological signals and physiological signal changes related to BG levels have high individual differences owing to the different responses of BG homeostasis among individuals [23], [54], [55]. Similar results were also reported in other researchers' work [21], [22], [56]. By using the splitting method, the model could learn the common features of different individuals and unique features of everyone at different BG levels automatically, which is helpful to overcome the limits of interindividual variability in ECG/PPG morphology and improve the accuracy of BG monitoring. Furthermore, the splitting method has the potentials in practical applications, and it can also be available to solve other general benchmark datasets. In fact, before BG measurement, the precalibration is a conventional means for CGM devices [57]. For instance, the users are acquired to complete a calibration process to personalize the device last for one week when they perform the noninvasive BG measurement [58]. Thus, in the future application, we first need to get part signals of everyone in other general benchmark data sets, and then, those signals were used for training and precalibration in the model. After training and precalibration, the model can achieve a high accuracy for noninvasive monitoring.

In comparison with some existing machine learning algorithms, such as gradient boost, random forest, and bagging, the average RMSE and MARD of the proposed fusion approach were the smallest, proving the feasibility and efficiency of the proposed approach. The reasons might be associated with weight-based Choquet integral multimodel fusion. Considering that every BG monitoring model (algorithm) has its own subject, it might work well for one but poorly for another individual at different time periods. Meanwhile, there is no sharp fluctuation of BG in a short time due to the homeostasis. In other words, there is a causal correlation between BG values at different time points. Hence, the BG value of each model was fused, respectively, based on the BG historical prediction values and BG current prediction value by using Choquet integral, which is helpful to avoid a single point of failure.

Furthermore, all the models were fused based on different weights, which will improve the BG monitoring accuracy.

Our study is only a first step toward noninvasive BG monitoring by fusing ECG and PPG signals. Despite this approach's potential clinical significance, there are two limitations of this study that need to be noted. First, the participants enrolled in this study were Asians. A further study of larger participants is warranted to confirm the validity of our proposed approach in different populations. Second, heart disease and blood diseases may cause the changes of ECG and PPG signals. The influence of different diseases on BG monitoring is not considered in this article.

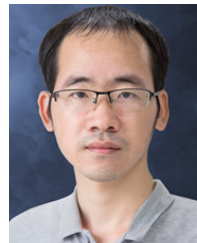
## VI. CONCLUSION

In this article, we proposed a new approach using ECG and PPG spatiotemporal features fusion and weight-based Choquet integral multimodel approach to achieve BG monitoring. The proposed approach consisted of three different fusion levels in this study. The first level was data fusion. The ECG and PPG signals were collected and fused into different pools. The second level was multilevel feature fusion. A total of 160 temporal statistical features were extracted from ECG and PPG signals. To find several suitable features, the candidate features were ranked by using three feature selection methods. In addition, there are 66 560 spatial morphological features acquired from ResNets automatically. To achieve spatial morphological features compression and fusion, the DNN was presented in our work. Forty spatial morphological features were obtained from the hidden layer of DNN. The third level was decision-level fusion. More specifically, the strategy of weight-based Choquet integral multimodel fusion was adopted at this level. The results indicated that the proposed approach has the excellent performance in comparison with several existing algorithms. In the near future, further studies with a larger number of normal individuals and diabetic individuals by continuous, long-term tracking of ECG/PPG and BG changes are warranted to validate our proposed model. In addition, we will explore the influence of different issues (e.g., motion artifacts) on BG monitoring in real-life conditions. We will leverage adaptive filtering technology and motion sensors to improve the accuracy of model.

## REFERENCES

- [1] A. Merovci et al., "Effect of mild physiologic hyperglycemia on insulin secretion, insulin clearance, and insulin sensitivity in healthy glucose-tolerant subjects," *Diabetes*, vol. 70, no. 1, pp. 204–213, Jan. 2021.
- [2] H. Sun et al., "IDF diabetes atlas: Global, regional and country-level diabetes prevalence estimates for 2021 and projections for 2045," *Diabetes Res. Clin. Pract.*, vol. 183, Jan. 2022, Art. no. 109119.
- [3] C. M. Lara-Rojas, L. M. Pérez-Belmonte, M. D. López-Carmona, R. Guijarro-Merino, M. R. Bernal-López, and R. Gómez-Huelgas, "National trends in diabetes mellitus hospitalization in Spain 1997–2010: Analysis of over 5.4 millions of admissions," *Eur. J. Internal Med.*, vol. 60, pp. 83–89, Feb. 2019.
- [4] T. Battelino et al., "Clinical targets for continuous glucose monitoring data interpretation: Recommendations from the international consensus on time in range," *Diabetes Care*, vol. 42, no. 8, pp. 1593–1603, Jun. 2019.
- [5] W. V. Gonzales, A. Mobashsher, and A. Abbosh, "The progress of glucose monitoring—A review of invasive to minimally and non-invasive techniques, devices and sensors," *Sensors*, vol. 19, no. 4, p. 800, Feb. 2019.
- [6] G. Cappon, M. Vettoretti, G. Sparacino, and A. Facchinetto, "Continuous glucose monitoring sensors for diabetes management: A review of technologies and applications," *Diabetes Metabolism J.*, vol. 43, no. 4, p. 383, 2019.
- [7] T. Lin, "Non-invasive glucose monitoring: A review of challenges and recent advances," *Current Trends Biomed. Eng. Biosci.*, vol. 6, no. 5, pp. 1–8, Jul. 2017.
- [8] Y. Chen et al., "Skin-like biosensor system via electrochemical channels for noninvasive blood glucose monitoring," *Sci. Adv.*, vol. 3, no. 12, Dec. 2017, Art. no. e1701629.
- [9] V. P. Rachim and W.-Y. Chung, "Wearable-band type visible-near infrared optical biosensor for non-invasive blood glucose monitoring," *Sens. Actuators B, Chem.*, vol. 286, pp. 173–180, May 2019.
- [10] M. C. Cebedio, L. A. Rabiglio, I. E. Gelosi, R. A. Ribas, A. J. Uriz, and J. C. Moreira, "Analysis and design of a microwave coplanar sensor for non-invasive blood glucose measurements," *IEEE Sensors J.*, vol. 20, no. 18, pp. 10572–10581, Sep. 2020.
- [11] S. Meyhofer et al., "Evaluation of a near-infrared light ultrasound system as a non-invasive blood glucose monitoring device," *Diabetes Obes. Metab.*, vol. 22, no. 4, pp. 694–698, Apr. 2020.
- [12] M. O. Bekkink, M. Koeneman, B. E. de Galan, and S. J. Bredie, "Early detection of hypoglycemia in type 1 diabetes using heart rate variability measured by a wearable device," *Diabetes Care*, vol. 42, no. 4, pp. 689–692, Mar. 2019.
- [13] H. Kinnunen, A. Rantanen, T. Kenttä, and H. Koskimäki, "Feasible assessment of recovery and cardiovascular health: Accuracy of nocturnal HR and HRV assessed via ring PPG in comparison to medical grade ECG," *Physiological Meas.*, vol. 41, no. 4, May 2020, Art. no. 04NT01.
- [14] J. Lázaro, N. Reljin, M. Hossain, Y. Noh, P. Laguna, and K. H. Chon, "Wearable armband device for daily life electrocardiogram monitoring," *IEEE Trans. Biomed. Eng.*, vol. 67, no. 12, pp. 3464–3473, Dec. 2020.
- [15] M. Ghamari, "A review on wearable photoplethysmography sensors and their potential future applications in health care," *Int. J. Biosensors Bioelectron.*, vol. 4, no. 4, p. 195, 2018.
- [16] S. H. Ling, P. P. San, and H. T. Nguyen, "Non-invasive hypoglycemia monitoring system using extreme learning machine for type 1 diabetes," *ISA Trans.*, vol. 64, pp. 440–446, Sep. 2016.
- [17] J. A. Lipponen et al., "Hypoglycemia detection based on cardiac repolarization features," in *Proc. Annu. Int. Conf. IEEE Eng. Med. Biol. Soc.*, Aug. 2011, pp. 4697–4700.
- [18] G. Zhang et al., "A noninvasive blood glucose monitoring system based on smartphone PPG signal processing and machine learning," *IEEE Trans. Ind. Informat.*, vol. 16, no. 11, pp. 7209–7218, Nov. 2020.
- [19] S. K. Khare and V. Bajaj, "Time-frequency representation and convolutional neural network-based emotion recognition," *IEEE Trans. Neural Netw. Learn. Syst.*, vol. 32, no. 7, pp. 2901–2909, Jul. 2021.
- [20] S. Wang, H. Tang, B. Wang, and J. Mo, "A novel approach to detecting muscle fatigue based on sEMG by using neural architecture search framework," *IEEE Trans. Neural Netw. Learn. Syst.*, early access, Nov. 9, 2021, doi: [10.1109/TNNLS.2021.3124330](https://doi.org/10.1109/TNNLS.2021.3124330).
- [21] M. Porumb, S. Stranges, A. Pescapè, and L. Pecchia, "Precision medicine and artificial intelligence: A pilot study on deep learning for hypoglycemic events detection based on ECG," *Sci. Rep.*, vol. 10, no. 1, pp. 1–16, Jan. 2020.
- [22] M. Porumb, C. Griffen, J. Hattersley, and L. Pecchia, "Nocturnal low glucose detection in healthy elderly from one-lead ECG using convolutional denoising autoencoders," *Biomed. Signal Process. Control*, vol. 62, Sep. 2020, Art. no. 102054.
- [23] J. Li, I. Tobore, Y. Liu, A. Kandwal, L. Wang, and Z. Nie, "Non-invasive monitoring of three glucose ranges based on ECG by using DBSCAN-CNN," *IEEE J. Biomed. Health Informat.*, vol. 25, no. 9, pp. 3340–3350, Sep. 2021.
- [24] K. Hu et al., "Graph fusion network-based multimodal learning for freezing of gait detection," *IEEE Trans. Neural Netw. Learn. Syst.*, vol. 34, no. 3, pp. 1588–1600, Mar. 2023.
- [25] Z. Ma, B. Sun, and S. Li, "A two-stage selective fusion framework for joint intent detection and slot filling," *IEEE Trans. Neural Netw. Learn. Syst.*, early access, Sep. 14, 2022, doi: [10.1109/TNNLS.2022.3202562](https://doi.org/10.1109/TNNLS.2022.3202562).
- [26] G. Tian et al., "Adding before pruning: Sparse filter fusion for deep convolutional neural networks via auxiliary attention," *IEEE Trans. Neural Netw. Learn. Syst.*, early access, Sep. 2021, doi: [10.1109/TNNLS.2021.3106917](https://doi.org/10.1109/TNNLS.2021.3106917).
- [27] R. Dian, S. Li, and X. Kang, "Regularizing hyperspectral and multispectral image fusion by CNN denoiser," *IEEE Trans. Neural Netw. Learn. Syst.*, vol. 32, no. 3, pp. 1124–1135, Mar. 2021.

- [28] D. X. Guo, Y. Z. Shang, R. Peng, S. S. Yong, and X. A. Wang, "Noninvasive blood glucose measurement based on NIR spectrums and double ANN analysis," *J. Biosci. Med.*, vol. 3, no. 6, pp. 42–48, 2015.
- [29] T. Tajima, Y. Tanaka, M. Nakamura, and M. Seyama, "Multi-modality analysis of glucose aqueous solution using photoacoustic and dielectric spectroscopy for non-invasive glucose monitoring," *Proc. SPIE*, vol. 10064, Mar. 2017, Art. no. 1006445.
- [30] K. Song, U. Ha, S. Park, J. Bae, and H. Yoo, "An impedance and multi-wavelength near-infrared spectroscopy IC for non-invasive blood glucose estimation," *IEEE J. Solid-State Circuits*, vol. 50, no. 4, pp. 1025–1037, Apr. 2015.
- [31] E. H. Houssein, M. Kilany, and A. E. Hassani, "ECG signals classification: A review," *Int. J. Intell. Eng. Inform.*, vol. 5, no. 4, pp. 376–396, 2017.
- [32] M. A. Motin, C. K. Karmakar, and M. Palaniswami, "Selection of empirical mode decomposition techniques for extracting breathing rate from PPG," *IEEE Signal Process. Lett.*, vol. 26, no. 4, pp. 592–596, Apr. 2019.
- [33] S. Sharma and S. Chaudhury, "Block sparse variational Bayes regression using matrix variate distributions with application to SSVEP detection," *IEEE Trans. Neural Netw. Learn. Syst.*, vol. 33, no. 1, pp. 351–365, Jan. 2022.
- [34] Y. Huang, G. G. Yen, and V. S. Tseng, "Snippet policy network V2: Knee-guided neuroevolution for multi-lead ECG early classification," *IEEE Trans. Neural Netw. Learn. Syst.*, early access, Jul. 11, 2022, doi: 10.1109/TNNLS.2022.3187741.
- [35] B. Sun, Z. Luo, and J. Zhou, "Comprehensive elaboration of glycemic variability in diabetic macrovascular and microvascular complications," *Cardiovascular Diabetol.*, vol. 20, no. 1, pp. 1–13, Jan. 2021.
- [36] R. Kher, "Signal processing techniques for removing noise from ECG signals," *J. Biomed. Eng. Res.*, vol. 3, pp. 1–9, Mar. 2019.
- [37] S. Kiliçkaya, A. Guner, and B. Dal, "Comparison of different machine learning techniques for the cuffless estimation of blood pressure using PPG signals," in *Proc. Int. Congr. Human-Comput. Interact., Optim. Robotic Appl. (HORA)*, Jun. 2020, pp. 1–6.
- [38] A. Jain, M. Singh, and B. Singh, "Real time system on chip based wearable cardiac activity monitoring sensor," *Meas., Sensors*, vol. 24, Dec. 2022, Art. no. 100523.
- [39] M. A. Hall, "Correlation-based feature selection for machine learning," Ph.D. dissertation, Dept. Comput. Sci., Univ. Waikato, Hamilton, New Zealand, 1999.
- [40] J. Li et al., "Towards noninvasive and fast detection of glycated hemoglobin levels based on ECG using convolutional neural networks with multisegments fusion and varied-weight," *Exp. Syst. Appl.*, vol. 186, Dec. 2021, Art. no. 115846.
- [41] K. He, X. Zhang, S. Ren, and J. Sun, "Identity mappings in deep residual networks," in *Proc. ECCV*, Amsterdam, The Netherlands, 2016, pp. 630–645.
- [42] M. Islam, D. T. Anderson, A. J. Pinar, T. C. Havens, G. Scott, and J. M. Keller, "Enabling explainable fusion in deep learning with fuzzy integral neural networks," *IEEE Trans. Fuzzy Syst.*, vol. 28, no. 7, pp. 1291–1300, Jul. 2020.
- [43] M. Calasan, S. H. A. Aleem, and A. F. Zobaa, "On the root mean square error (RMSE) calculation for parameter estimation of photovoltaic models: A novel exact analytical solution based on Lambert W function," *Energy Conv. Manag.*, vol. 210, Apr. 2020, Art. no. 112716.
- [44] S. Yoshino et al., "Assessment of factors that determine the mean absolute relative difference in flash glucose monitoring with reference to plasma glucose levels in Japanese subjects without diabetes," *Endocrine J.*, vol. 67, no. 5, pp. 537–544, 2020.
- [45] N. Dunne, M. T. Viggiani, S. Pardo, C. Robinson, and J. L. Parkes, "Accuracy evaluation of CONTOUR PLUS compared with four blood glucose monitoring systems," *Diabetes Therapy*, vol. 6, no. 3, pp. 377–388, Jul. 2015.
- [46] J. Chamberlain, "Continuous glucose monitoring systems: Categories and features," *ADA Clin. Compendia*, vol. 2018, pp. 8–10, Aug. 2018.
- [47] G. Freckmann, S. Pleus, M. Grady, S. Setford, and B. Levy, "Measures of accuracy for continuous glucose monitoring and blood glucose monitoring devices," *J. Diabetes Sci. Technol.*, vol. 13, no. 3, pp. 575–583, May 2019.
- [48] C. Zhang et al., "Video based cocktail causal container for blood pressure classification and blood glucose prediction," *IEEE J. Biomed. Health Informat.*, vol. 27, no. 2, pp. 1118–1128, Feb. 2023.
- [49] D. U. Uguz, T. B. Tufan, A. Uzun, S. Leonhardt, and C. H. Antink, "Physiological motion artifacts in capacitive ECG: Ballistocardiographic impedance distortions," *IEEE Trans. Instrum. Meas.*, vol. 69, no. 6, pp. 3297–3307, Jun. 2020.
- [50] R. Carnagarin, V. B. Matthews, L. Y. Herat, J. K. Ho, and M. P. Schlaich, "Autonomic regulation of glucose homeostasis: A specific role for sympathetic nervous system activation," *Current Diabetes Rep.*, vol. 18, no. 11, pp. 1–10, Sep. 2018.
- [51] H. Lee, J. Lee, and M. Shin, "Using wearable ECG/PPG sensors for driver drowsiness detection based on distinguishable pattern of recurrence plots," *Electronics*, vol. 8, no. 2, p. 192, Feb. 2019.
- [52] J. R. Pinto, J. S. Cardoso, and A. Lourenço, "Evolution, current challenges, and future possibilities in ECG biometrics," *IEEE Access*, vol. 6, pp. 34746–34776, 2018.
- [53] T. Rao, X. Li, H. Zhang, and M. Xu, "Multi-level region-based convolutional neural network for image emotion classification," *Neurocomputing*, vol. 333, pp. 429–439, Mar. 2019.
- [54] I. Tobore, J. Li, A. Kandwal, L. Yuhang, Z. Nie, and L. Wang, "Statistical and spectral analysis of ECG signal towards achieving non-invasive blood glucose monitoring," *BMC Med. Informat. Decis. Making*, vol. 19, no. 6, pp. 1–14, Dec. 2019.
- [55] T. Igbe et al., "Analysis of ECG segments for non-invasive blood glucose monitoring," in *Proc. IEEE Int. Conf. E-Health Netw., Appl. Services (HealthCom)*, Bogota, Colombia, Oct. 2019, pp. 1–6.
- [56] J. A. Lipponen et al., "Dynamic estimation of cardiac repolarization characteristics during hypoglycemia in healthy and diabetic subjects," *Physiolog. Meas.*, vol. 32, no. 6, pp. 649–660, Apr. 2011.
- [57] S. A. Siddiqui, Y. Zhang, J. Lloret, H. Song, and Z. Obradovic, "Pain-free blood glucose monitoring using wearable sensors: Recent advancements and future prospects," *IEEE Rev. Biomed. Eng.*, vol. 11, pp. 21–35, 2018.
- [58] Y. Segman, "Device and method for noninvasive glucose assessment," *J. Diabetes Sci. Technol.*, vol. 12, no. 6, pp. 1159–1168, Nov. 2018.



**Jingzhen Li** (Member, IEEE) received the B.E. and M.Sc. degrees from the College of Electronic Science and Technology, Shenzhen University, Shenzhen, China, in 2011 and 2014, respectively.

He is currently a Research Associate with the Shenzhen Institute of Advanced Technology, Chinese Academy of Sciences, Shenzhen. He has published over 25 international journals and conference papers in IEEE, Nature, Elsevier, and Wiley. Also, he has filed more than 20 patents. His research interests include deep learning and blood glucose monitoring.



**Jingjing Ma** received the B.S. degree from the Wuhan University of Science and Technology, Wuhan, China, in 2004, and the master's degree from the Wuhan University of Technology, Wuhan, in 2007.

She is currently a Senior Engineer with the Testing and Technology Center for Industrial Products of Shenzhen Customs, Shenzhen, China. She has authored more than 20 scientific articles, one book chapters, and filed ten patents. Her research interests include signal monitoring and data analysis.



**Olatunji Mumini Omisore** (Senior Member, IEEE) received the Ph.D. degree in pattern recognition and intelligent systems from the University of Chinese Academy of Sciences, Beijing, China, in 2019.

He has worked as a Software Engineer, a System Analyst, and a Lecturer in three different higher institutions. He currently works as a Research Associate Professor on medical robotics and MIS devices with the Shenzhen Institute of Advanced Technology, Chinese Academy of Sciences, Shenzhen, China. He has authored or coauthored more than 60 articles in top-ranked journal and conference venues. He has experience leading and participating in major research projects funded by national and international grant bodies, such as the Key National Natural Science Foundations of China. His research interests include learning-based constraints control in flexible surgical robotics, computational intelligence, and digital libraries with specialty in data and knowledge mining.



**Yan Yan** (Member, IEEE) received the B.Eng. and M.Sc. degrees in instrument engineering from the Harbin Institute of Technology, Harbin, China, in 2010 and 2012, respectively, and the Ph.D. degree in computer science from the University of Chinese Academy of Sciences, Beijing, China, in 2020.

He worked as a Research Assistant at the Shenzhen Institutes of Advanced Technology, Chinese Academy of Sciences, Shenzhen, China, from 2012 to 2014. He also worked with the Department of Computer Science, University of Liverpool, Liverpool, U.K., as an Honorary Research Assistant, from 2017 to 2018, advised by Prof. Yannis Goulermas. He is currently a Research Associate with the Shenzhen Institutes of Advanced Technology, Chinese Academy of Sciences. His research interests include biomedical signal processing, machine learning, nonlinear dynamical systems, and topological data analysis.



**Yuhang Liu** received the B.Sc. and M.Sc. degrees from Yunnan University, Kunming, China, in 2012 and 2015, respectively.

She is currently an Engineer with the Shenzhen Institute of Advanced Technology, Chinese Academy of Sciences, Shenzhen, China. Her research interests include human body communication for body sensor network and feature extraction from physiological signal.



**Huajie Tang** received the B.E. degree from the Tianjin University of Technology and Education, Tianjin, China, in 2011, and the M.Sc. degree from Guizhou University, Guiyang, China, in 2014.

He is currently an Engineer with the Shenzhen Institute of Advanced Technology, Chinese Academy of Sciences, Shenzhen, China. His research interests include microwave, mm-wave, and biomedical engineering.



**Lei Wang** (Member, IEEE) received the B.S. degree in information and control engineering and the Ph.D. degree in biomedical engineering from Xi'an Jiaotong University, Xi'an, China, in 1995 and 2000, respectively.

From 2001 to 2008, he was with the University of Glasgow, Glasgow, U.K., and the Imperial College London, London, U.K. He is now at the Shenzhen Institute of Advanced Technology, Chinese Academy of Sciences, Shenzhen, China, as a Professor and the Center Director with the Medical Robotics and MIS Devices. He has authored more than 200 scientific papers, nine books/book chapters, and filed 60 patents. His research interests focus on body sensor networks and machine learning.



**Pengfei Ao** received the B.E. degree from the South China University of Technology, Guangzhou, China, in 2015, and the M.Sc. degree from Newcastle University, Newcastle upon Tyne, U.K., in 2017.

He is currently an Engineer with the Shenzhen Institute of Advanced Technology, Chinese Academy of Sciences, Shenzhen, China. His research interests include algorithm framework, signal processing, and embedded engineering.



**Zedong Nie** (Member, IEEE) received the M.Sc. degree from the Wuhan University of Science and Technology, Wuhan, China, in 2007, and the Ph.D. degree from the University of Chinese Academy of Sciences, Beijing, China, in 2013.

He is currently a Professor with the Shenzhen Institute of Advanced Technology, Chinese Academy of Sciences, Shenzhen, China. He has published over 50 papers in IEEE, Nature, Elsevier, and Wiley. His research interests include short-range communication, wearable technology, body sensor network, and medical electronics.